

Do Large Scale Molecular Language Representations Capture Important Structural Information?

Jerret Ross^{1,*}, Brian Belgodere¹, Vijil Chenthamarakshan¹, Inkit Padhi¹, Youssef Mroueh¹, and Payel Das^{1,*}

¹IBM Research, Yorktown Heights, NY 10598, USA

*rossja@us.ibm.com and daspa@us.ibm.com

ABSTRACT

Predicting the chemical properties of a molecule is of great importance in many applications, including drug discovery and material design. Machine learning based molecular property prediction holds the promise of enabling accurate predictions at much less computationally complex cost when compared to, for example, Density Functional Theory (DFT) calculations. Various representation learning methods in a supervised setting, including the features extracted using graph neural nets, have emerged for such tasks. However, the vast chemical space and the limited availability of labels make supervised learning challenging, calling for learning a general-purpose molecular representation. Recently, pre-trained transformer-based language models on large unlabeled corpus have produced state-of-the-art results in many downstream natural language processing tasks. Inspired by this development, we present molecular embeddings obtained by training an efficient transformer encoder model, MoLFormer. This model employs a linear attention mechanism coupled with highly parallelized training on SMILES sequences of 1.1 billion unlabeled molecules from the PubChem and ZINC datasets. Experiments show that the learned molecular representation outperforms supervised and unsupervised graph neural net baselines on several regression and classification tasks from 10 benchmark datasets, while performing competitively on others. Further analyses, specifically through the lens of attention, demonstrate that MoLFormer indeed learns a molecule's local and global structural aspects. These results provide encouraging evidence that large-scale molecular language models can capture sufficient structural information to be able to predict diverse molecular properties, including quantum-chemical properties.

1 Introduction

Machine learning (ML) has emerged as an appealing alternative for predicting molecular properties as a computationally efficient approach, with implications in drug discovery, quantum chemistry, and material design.

ML models for molecules can be trained directly on a set of pre-defined chemical descriptors, such as unsupervised molecular fingerprints¹, or hand-derived derivatives of geometric features such as Coulomb Matrix (CM)². More recent ML models have focused on automatically learning the features either from the natural graphs that encode the connectivity information or from the line annotations of molecular structures, such as the popular SMILES (simplified molecular-input line entry system) representation³. SMILES defines a character string representation of a molecule by performing a depth-first pre-order traversal of a spanning tree of the molecular graph, generating symbols for each atom, bond, tree-traversal decision, and broken cycles. Therefore, the resulting character string corresponds to a flattening of a spanning tree of the molecular graph. Learning on SMILES has been widely adopted for molecular property prediction⁴⁻⁷, as SMILES is generally more compact than other methods of representing structure, including graphs. Additionally, meaningful substructures such as branches, cyclic structures, and chirality information are explicitly represented in SMILES strings, which is not the case for the graph representation.

However, the SMILES grammar is complex and restrictive; most sequences over the appropriate character set do not belong to well-defined molecules. Alternative string-based representations exist, such as SMARTS⁸ and SELFIES⁹. Nevertheless, string-based representations are thought not to be topology-aware while graphs are. Due to these limitations, deep models may focus their learning on the grammar of molecular strings and not the implicit topological structure. Accordingly, while string-based deep neural nets have been employed in predicting the physico/bio-chemical properties^{5-7,10}, their ability toward predicting quantum-mechanical (QM) properties, that are strongly tied to a low energy 3D structure (also referred to as conformer), has been less explored.

In contrast, Graph Neural Networks (GNNs)¹¹ and their variants including¹²⁻²⁰ have been extensively used and shown impressive performance for learning molecular representations on QM property prediction. GNN frameworks can be generally

viewed as “message passing”, which includes local neighborhood information aggregation and information update across different levels of granularity, e.g., nodes, edges, or the full graph, according to the graph’s connectivity structure.

Label annotation of molecules is typically expensive, while the size of the space consisting of plausible chemicals is astronomically large (10^{60-100})²¹. Such a scenario naturally evokes for molecular representation learning in an unsupervised setting, which can be generalizable to a variety of property prediction tasks. Recent success of language representation models (LM) in downstream NLP tasks, as obtained by combining the power of pre-training on large unlabeled corpus and contextual LMs using advanced neural nets like Transformers²², has inspired extending this paradigm to other domains, where domain-specific “language” embeddings obtained using pre-trained LMs were exploited as the exclusive input for several subsequent tasks. Only recently, pre-trained LMs²³ and GNNs²⁴ started to emerge for molecular property predictions.

Here we present transformer models of molecular SMILES, obtained using efficient linear attention mechanism and trained on a large corpus of 1.1 billion molecules, referred as MOLFORMER (Molecular Language transformer). Results show, for the first time, that pre-trained transformer encoders of molecular SMILES perform competitively with existing supervised or unsupervised LM and GNN baselines on predicting a wide variety of molecular properties, including quantum-mechanical ones.

Our main contributions are

- We train a large-scale and efficient Molecular Language model transFormer (MOLFORMER) on over a billion molecules, with relatively limited hardware resources (up to 16 V100 GPUs). We owe our scalability and speedups to efficient linear time attention, adaptive bucketing of batches, and open-source parallelization provided in PyTorch Lightning and NCCL. Without the combination of bucketing and linear attention, we would be limited to a batch size of less than 50 per GPU, requiring us to use over 1000 GPUs to achieve the same wall clock time.
- We explore the difference between absolute and relative position embeddings in representing molecular SMILES. We also provide a new, efficient, and accurate linear attention approximation of the recently proposed relative position Roformer.
- We perform extensive experimentation and ablation studies on several classification and regression tasks from 10 benchmark datasets, including quantum mechanical, physical, biophysical, and physiological property prediction.
- Our results provide encouraging evidence that MOLFORMER representations can capture sufficient structural information to predict a diverse range of chemical properties accurately. Furthermore, the performance of MOLFORMER is either better or on par with state-of-the-art GNNs that learn from precise graph topology information and beyond (e.g., bond distances).
- We provide further analyses to demonstrate that MOLFORMER can capture substructures and bond connectivity within a molecule from SMILES annotations.

2 Related Work

Large Scale Training of Language Model The recent advancement of transformer-based masked language models (MLMs)^{25,26} and prefix language models (PLMs)²⁷ have shown remarkable performance on various natural language understanding tasks. Unsupervised pre-trained representation learning of sequences through MLMs randomly masks input tokens during training and then predicts these masked tokens. Whereas PLMs require adding task-specific text tags to the input sequences. These language models show substantial scalability through increasing transformer models size and training using large-scale data corpora. Moreover, recent efforts to address the challenges of memory usage and costs incurred in modeling long-range dependencies as sequence length increases. Different efficient transformers introduced through²⁸⁻³¹ address the quadratic memory challenges within the self-attention mechanism.

Molecular Representation Learning To represent molecules in vector space, traditional chemical fingerprints such as ECFP¹, have been used. Deep neural nets were further trained on chemical fingerprints for supervised learning. RNN-based models have been used for molecular representation learning using SMILES and other linear molecular annotations as inputs³². At the same time, graph convolutional layers have been used to learn the neural fingerprints of molecules^{11,33,17}. implemented a single common framework to learn from graphs, referred as message passing framework, which computes node embeddings by aggregating neighbor hood information during message passing phase and computes a feature vector of the graph during the readout phase. Many attempts on extending GNNs have been made to variations of the original message passing concept aimed at learning non-local effects; for instance,³⁴ introduced an attention mechanism. One challenge faced by GNNs is achieving higher expressivity that can distinguish between two given graphs to that of the hierarchy of the Weisfeiler-Lehman (WL) graph isomorphism, while maintaining scalability. It has been shown that typical message passing models have limited expressiveness and are not better than the first WL test (1-WL)³⁵. Powerful deep models that represent higher order interactions between graph nodes have been suggested^{35,36}, at the cost of high computational expense.

Molecular graphs can have additional access to 3D information. To better capture the spatial interactions among atoms,¹⁷ extended the message passing framework to include pairwise interatomic distances as edge features. More recently, variations of the message passing networks (MPNN) were proposed to better model the spatial interactions within molecules and to increase the expressive power of models e.g., by using continuous filter convolutional layers³⁷ or by using directional message passing³⁸, at the cost of increased computational complexity. However, those models are not generalizable to settings where 3D structural information is not readily available and/or expensive to compute (e.g. for bigger molecules). Since the goal of this work is to learn a generalizable molecular representation from large amount of unlabeled data without relying on expensive 3D information, we mainly focus on comparing the proposed molecular language model with existing supervised and un/self-supervised baselines that utilizes different input representation (SMILES, graphs, fingerprints) and can be generalizable to a wide variety of tasks, from quantum mechanical to physiological.

Pre-trained Molecular Language and Graph Models Recent success of language representation models in downstream NLP tasks, as obtained by combining the power of pre-training on large unlabeled corpus and contextual language models (LMs) using advanced neural nets like Transformers, has inspired extending this paradigm to other domains, where a domain-specific “language” embeddings obtained using PTMs were exploited as the exclusive input for several subsequent tasks. One such example is understanding the language of life through advanced LMs trained on protein sequences, in which features extracted by LMs directly from single protein sequences reach state-of-the art performance in downstream prediction tasks, even when those were used without evolutionary information^{39–41}. Similar large-scale unsupervised pre-training on SMILES sequences has been explored for molecular property prediction^{23,42,43}; however, those models did not attempt to predict quantum chemical properties. Unsupervised/self-supervised representation learning has been tested on molecular graphs as well^{24,44,45}. To our knowledge, the present study is the first one that explores the representational power of pre-trained molecular language models on predicting downstream quantum mechanical targets for which learning the molecular structural information is known to be crucial.

3 Large-scale and Efficient Pretrained Molecular Language Models

Datasets and Tokenization The dataset that we use for pretraining is a combination of the PubChem⁴⁶ and ZINC⁴⁷ databases. PubChem consists of 111 million molecules, while the much larger ZINC dataset contains of around 1 billion molecules. To construct a vocabulary, we utilize the tokenizer from⁴⁸. Running this tokenizer on molecules converted to the canonical form utilizing RDKit, we end up with a vocabulary size of 2357 characters plus 5 special characters, totalling up to 2362 characters for the combined PubChem+ZINC. The sequence length of the molecules after tokenization range from 1 to just over 2000 characters. We decide to limit our sequence length range from 1 character to 202 characters, special characters inclusive, to reduce computation time. We assumed that this would have minimal impact on training due to over 99.4 percent of all molecules from our dataset containing less than 202 characters.

3.1 Efficient Transformer Encoder with Linear Attention

One of the computational bottlenecks in transformers²² is the attention mechanism with a quadratic computational cost with respect to sequence length. Linear complexity attention models^{28,49} tackled this issue, via kernel approximations using variants of random feature approximations.

Aiming at training large scale Masked Language Models efficiently utilizing relatively limited hardware resources, we decided to experiment with an encoder transformer with Linear attention⁴⁹. Our model consists of 12 layers, 12 attention heads per layer and has a hidden state size of 768. A Generalized Feature map⁴⁹ for the linear attention was chosen after preliminary experiments showed an acceptable balance between computation speedup and minimal performance reduction when compared to the FAVOR²⁸ feature map. Generalized features are a simplification of the feature map in FAVOR²⁸. The Generalized map removes the softmax approximation but it can increase the rank of the resulting attention matrix. The size of the feature map is 32.

3.2 Position Embeddings and Fast Linear RoFormer

The seminal work of²² considered absolute position embeddings to encode the position of a token in the sequence.^{50–52} showed that using relative position embeddings between tokens results in better performance. Rotary position embeddings were introduced recently in RoFormer of⁵³ as a means to enhance relative encoding via position dependent rotations R_m of the query and the keys at a position m . These rotations can be efficiently implemented as pointed-wise multiplications and do not result in cumbersome computations.

In order to leverage Rotary embeddings with linear transformers,⁵³ proposed the use of the following approximation :

$$\text{Attention}_m(Q, K, V) = \frac{\sum_{n=1}^N \langle R_m \phi(q_m), R_n \phi(k_n) \rangle v_n}{\sum_{n=1}^N \langle \phi(q_m), \phi(k_n) \rangle},$$

where Q, K, V are the query, key and value respectively, and φ a random feature map.

After a preliminary experimentation with this fast Roformer, we found it to be behind its absolute position counterpart. We propose the following linear attention for Roformer that we found to train gracefully:

$$\text{Attention}_m(Q, K, V) = \frac{\sum_{n=1}^N \langle \varphi(R_m q_m), \varphi(R_n k_n) \rangle v_n}{\sum_{n=1}^N \langle \varphi(R_m q_m), \varphi(R_n k_n) \rangle}.$$

When compared with⁵³ we rotate the original keys and queries instead of the transformed ones with the feature map φ . We saw increased stability and faster convergence in training loss behavior on both PubChem and PubChem+ZINC when using rotary embeddings over absolute embeddings as observed in Figure 1(a).

3.3 Large Scale Training and Parallelization

Masked LM Training For pretraining we use the masked language model method defined in²⁶, 80% of the time a character will be replaced with the mask token, 10% of the time the character will be replaced with a random character and 10% of the time the character will be unchanged. For optimization we decided to use the Fused Lamb optimizer from⁵⁴ as implemented via APEX. This decision was made due to Lamb’s superior performance in training. For example, learning rate warm ups were found to be unnecessary and training was found to be robust when large batch sizes were used. All other optimizers were unable to maintain their stability without large amounts of modification any time a training configuration needed to be changed. Training took place for 4 epochs through the entire PubChem+ZINC dataset with a fixed learning rate of $1.6e^{-4}$ and a batch size of 1600 molecules per GPU on a total of 16 GPUs over 2 servers connected via Infiniband fabric. It should be noted that as the number of GPUs utilized increased we found an increase in learning rate was necessary up to a factor of 8.

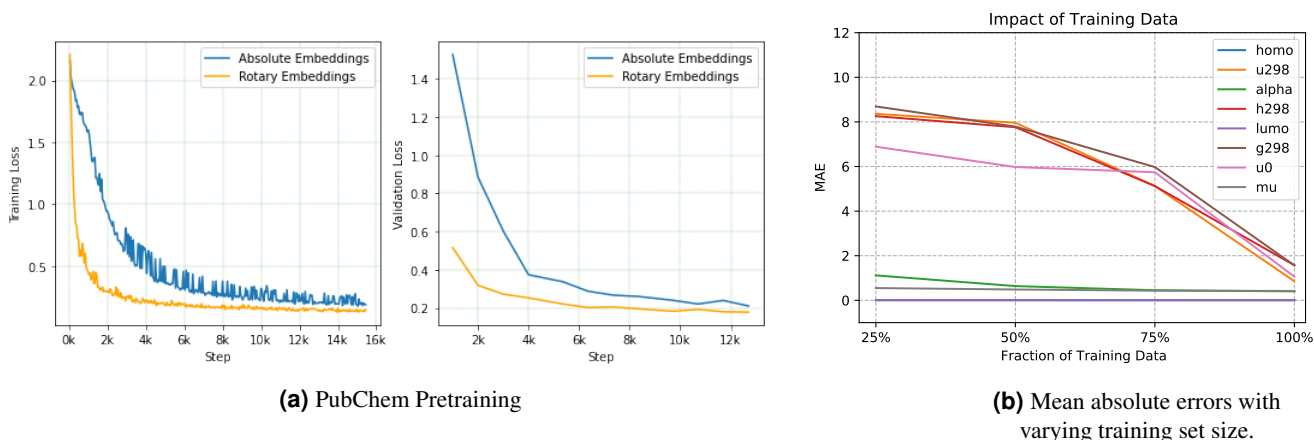


Figure 1. (a) Training and validation losses of our Linear attention MOLFORMER with *rotary* (relative) and absolute position embeddings on PubChem. We see that both rotary and absolute MOLFORMER have graceful training curves. Our Rotary Linear attention MOLFORMER leads to lower training and validation losses than MOLFORMER with absolute position embeddings. (b) Finetuning of MOLFORMER with rotary embeddings for prediction of various properties on QM9 Molecules for different training set sizes.

In order to scale our training to large datasets (1 Billion+ data points), we relied on adaptive bucketing of mini-batches by sequence length, as well as parallelization via distributed training (see Appendix B for details). Using Linear attention and bucketing allowed us to reduce the number of GPU needed for quadratic attention and no bucketing from roughly 1000 to 16.

4 Experimental Results

4.1 MoLFORMER embeddings

We encode a molecule by extracting the average embedding from the encoder model. The average embedding comes from the average of all embeddings of the last hidden state of the encoder model. For downstream tasks, we use this embedding. We employ two strategies for the downstream tasks – the first strategy (Frozen) is to train a fully connected model for each task while keeping the encoder embeddings fixed. The second strategy is to fine tune the weights of the encoder model jointly with the fully connected model for each downstream task. The ideal configuration and hyperparameters for the first strategy are identified through a grid search as described in the supplemental material. For the second strategy, we use a 2 layer fully

connected network with a hidden dimension of 768 (matching the encoder embedding) with Dropout (set to 0.1) and GELU layers in-between, on top of a final single output dimension for regression tasks.

4.2 Ablation Studies

We take in this section QM9 benchmark as a test-bed to perform ablation studies on MOLFORMER. The QM9 benchmark consists of 12 regression tasks, each consisting of approximately 134k organic molecules with up to nine heavy atoms from carbon, oxygen, nitrogen, and fluorine. We present here an ablation of MOLFORMER variants using absolute or rotary (relative) position embeddings that are pretrained on (1) only QM9 training set (111k) – referred as MOLFORMER-qm9 (2) only PubChem (111M) – referred as MOLFORMER-pubchem (3) PubChem+ZINC data (1.1 Billion +) – referred as MOLFORMER-XL.

We then train on top of MOLFORMER embeddings, as mentioned earlier a 2 layers MLP with 768 neurons each to predict various properties on the QM9 benchmark. MOLFORMER may be frozen in this setting or finetuned and trained along with the MLP. Due to space constraints, the results of this ablation of finetuned MOLFORMER variants trained on a random fixed split of the QM9 data (80% train, 10% test, and validation each) are given in appendix (Table 12 for MOLFORMER-qm9, Table 5 left/right for MOLFORMER-pubchem and MOLFORMER-XL). These results show that relative position embeddings (Rotary embeddings) and finetuning outperform other combinations using frozen or absolute embeddings. Hence when we refer to MOLFORMER in what follows, it is implicitly implied that it used rotary embeddings, unless specified otherwise. Moreover, the performance on downstream tasks based on average MAE varies in the following order: MOLFORMER-pubchem < MOLFORMER-qm9 < MOLFORMER-XL, confirming that unsupervised pre-training on a more extensive and diverse corpus enhances the representational power of the model, as showcased by its stronger performance on the QM9 benchmark.

In order to ensure the robustness of these results across data splits we also give, in the appendix, the performance of MOLFORMER variants on QM9 tasks using 5-cross validations folds (Table 6 for MOLFORMER-pubchem and Table 7 for MOLFORMER-XL). These results confirm the stability of the results and that MOLFORMER-XL outperforms other variants. Hence in the rest of the paper, we use MOLFORMER-XL on other molecular downstream tasks.

We further experimented with the effect of the finetuning datasize by training on portions on the QM9 data. In Figure 1(b), we see that the MAE is stable across portions of the finetuning data for some tasks (homo, lumo, mu). This stability is yet another benefit of MOLFORMER-XL that was pretrained on large amounts of data. For other tasks, the more data is available, the better finetuning performs.

	Graph-Based			Geometry-Based			SMILES-Based	
Measure	A-FP	123-gnn	GC	CM	DTNN	MPNN	MOLFORMER-XL	ChemBERTa
α	0.492	0.27	1.37	0.85	0.95	0.89	0.3327	0.8510
C_v	0.252	0.0944	0.65	0.39	0.27	0.42	0.1447	0.4234
G	0.893	0.0469	3.41	2.27	2.43	2.02	0.3362	4.1295
gap	0.00528	0.0048	0.01126	0.0086	0.0112	0.0066	0.0038	0.0052
H	0.893	0.0419	3.41	2.27	2.43	2.02	0.2522	4.0853
ϵ_{homo}	0.00358	0.00337	0.00716	0.00506	0.0038	0.00541	0.0029	0.0044
ϵ_{lumo}	0.00415	0.00351	0.00921	0.00645	0.0051	0.00623	0.0027	0.0041
μ	0.451	0.476	0.583	0.519	0.244	0.358	0.3616	0.4659
$\langle R^2 \rangle$	26.839	22.90	35.97	46.00	17.00	28.5	17.0620	86.150
U_0	0.898	0.0427	3.41	2.27	2.43	2.05	0.3211	3.9811
U	0.893	0.111	3.41	2.27	2.43	2.00	0.2522	4.3768
ZPVE	0.00207	0.00019	0.00299	0.00207	0.0017	0.00216	0.0003	0.0023
Avg MAE	2.6355	1.9995	4.3536	4.7384	2.3504	3.1898	1.5894	8.7067
Avg std MAE	0.0854	0.0658	0.1683	0.1281	0.1008	0.1108	0.0567	0.1413

Table 1. MOLFORMER performance on QM9 test set. Our best MOLFORMER variant is pretrained on PubChem+ZINC dataset and finetuned for each measure. Baseline performance values are taken from^{34,36,55}. Blue and Orange indicates best and second-best performing model, respectively. MOLFORMER trained with rotary embeddings on PubChem+ZINC achieves the best Avg MAE and Avg. std. MAE across all tasks.

4.3 Performance of MOLFORMER embeddings on Downstream Tasks

We evaluate the performance of MOLFORMER embeddings and compare with existing baselines on several downstream tasks, specifically five regression and six classification tasks from the MoleculeNet benchmark⁵⁵, as discussed below. First,

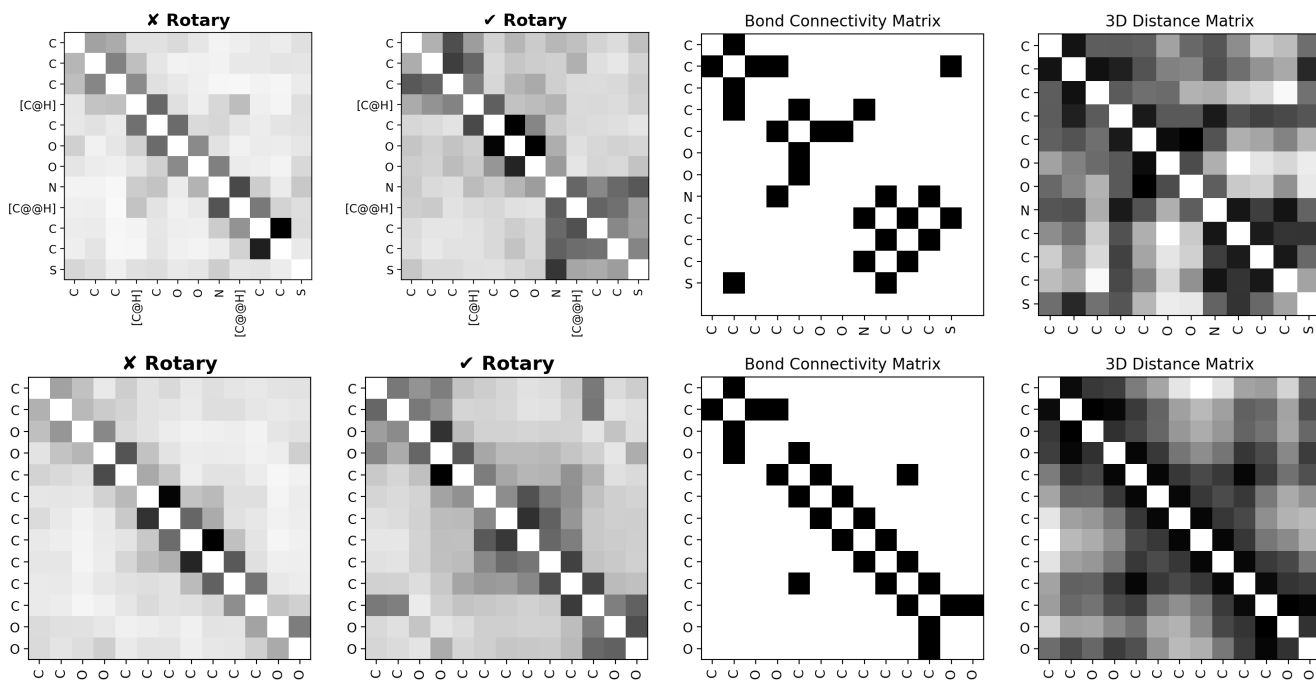


Figure 2. Visualization of the learned attention map (using either rotary or absolute position embedding) and corresponding molecular structure (bond connectivity and 3D distance) for two random molecules:

'CC1 (C) [C@H] (C (O)=O) N2 [C@@H] (CC2) S1' (top) and 'CC (=O) OC1=CC=CC=C1C (=O) O' (bottom). The attention map (only tokens that map to constituent atoms are shown for clarity), comprised of the average-pooled heads of an intermediate attention layer, exhibits awareness of both covalent bond connectivity and long-range spatial relationship.

Task	GC	A-FP	MPNN	MOLFORMER-XL
QM8 (avg MAE)	0.0148	0.0282	0.0143	0.0102
ESOL (RMSE)	0.97	0.503	0.58	0.2787
FreeSolv (RMSE)	1.40	0.736	1.15	0.2308
Lipophilicity (RMSE)	0.655	0.578	0.719	0.5289

Table 2. Performance of finetuned MOLFORMER and other supervised GNN baselines on QM8, ESOL, FreeSolv and Lipophilicity regression benchmarks. Baseline performances are taken from references^{34,55}.

Dataset	BBBP	Tox21	ClinTox	HIV	BACE	SIDER
Tasks	1	12	2	1	1	27
RF	71.4	76.9	71.3	78.1	86.7	68.4
SVM	72.9	81.8	66.9	79.2	86.2	68.2
MGCN ⁵⁶	85.0	70.7	63.4	73.8	73.4	55.2
D-MPNN ⁵⁷	71.2	68.9	90.5	75.0	85.3	63.2
Hu, et al. ⁵⁸	70.8	78.7	78.9	80.2	85.9	65.2
N-Gram ⁴⁴	91.2	76.9	85.5	83.0	87.6	63.2
MolCLR ²⁴	73.6	79.8	93.2	80.6	89.0	68.0
MOLFORMER-XL	93.7	84.7	94.8	82.2	88.21	69.0

Table 3. Comparison of MOLFORMER with existing supervised and pre-trained/self-supervised baselines on classification benchmarks. Baseline performances are adopted from²⁴.

we discuss the results on the popular QM9 benchmark. Here we choose existing baselines that fall in the following three classes: (1) Graph-based models that do not consider spatial information and learns only from topological information. In this category, we consider a molecular graph convolutional network (GC, a GNN that utilizes a mean-pooling over the node and

its neighbors before the linear transformation)⁵⁹, the attentive-FP (A-FP) model³⁴, and the 123-GNN model³⁵, a GNN that is more powerful than 1-WL. (2) An existing pre-trained molecular language model trained on a smaller chemical dataset²³. (3) Geometry-based models. Since for QM9 (and other similar quantum mechanical benchmarks), the 3D Cartesian coordinates of the most stable conformation is available for each molecular graph, learning on 3D spatial information has been found to provide a greater performance boost than learning on graph topology alone¹⁷. However, such 3D information is not broadly available, and learning on spatial information increases computational complexity. As the scope of this work is to derive a computationally efficient self-supervised molecular representation learning framework from readily available molecular information such as SMILES, which is generalizable to a wide variety of property prediction tasks, we refrain from comparing MOLFORMER with state-of-the-art GNNs that are specialized toward accurate modeling of quantum-mechanical interactions (e.g., DIMENet³⁸). Nevertheless, we still include relatively simpler DNN and GNN baselines that utilize interatomic spatial distances as auxiliary information to test the limit of MOLFORMER. These baselines include a multitask neural net encoding the Coulomb Matrix (CM)⁶⁰, its GNN variant as in the deep tensor neural net (DTNN)⁶¹, and an MPNN variant¹⁷ that learns edge features such as pairwise interatomic distances.

Results reported in Table 1 show that, though there is a consensus in the community that SMILES does not explicitly encode topological or geometric information, MOLFORMER with task-specific fine-tuning trained on SMILES strings of large molecular corpus achieves comparable or better performance to that of the majority of the competitors. Specifically, MOLFORMER outperforms all baselines in term of average MAE and average standard MAE. ChemBERTa shows the highest average MAE among all. More expressive 123-GNN performs better on most measures than MOLFORMER; however, such powerful networks are known to be difficult to scale (see⁶² for example). As a comparison, the linear attention employed in MOLFORMER ensures a linear time complexity.

To check the generalizability of MOLFORMER-XL, we report its performance on three other regression benchmarks, namely QM8, ESOL, FreeSolv, and Lipophilicity, in Table 2. We use a random 80%/10%/10% train/validation/test split as suggested in⁵⁵. Results show that MOLFORMER-XL upon task-specific fine-tuning outperforms the existing supervised GNN baselines, specifically GC, A-FP, and MPNN (augmented with bond distances for QM8 only), by a significant margin, confirming its generalizability. We further extend the comparison of MOLFORMER to a number of pre-trained/self-supervised molecular representation learning frameworks. Specifically, Hu, et al.⁵⁸ pre-trains a Graph Isomorphism Network (GIN, a GNN that uses an MLP and weighted sum of node features in the aggregation) on molecular graphs that includes edge features involved in aggregation. N-gram graph⁴⁴ uses a simple unsupervised representation for molecules by first embedding the nodes in a graph and then then constructing a compact representation of the graph by assembling the vertex embeddings in short walks in the graph. MolCLR²⁴ is a self-supervised learning framework based on GIN, which uses contrastive loss^{63,64}. Table 3 documents the performance comparison of MOLFORMER with these pretrained/self-supervised baselines on six classification benchmarks, while using scaffold data splits. Four supervised baselines are also shown, as reported in²⁴. Again, MOLFORMER-XL outperforms all baselines in four out of six benchmarks and comes second in the remaining two.

Correlation	ChemBERTa	MOLFORMER-XL
Fingerprint	0.48	0.64
MCS	-0.44	-0.60

Table 4. Correlation with structural similarity metrics. Reported correlations are between (1) the pairwise similarities estimated using molecular Fingerprints and those using MOLFORMER-XL (or ChemBERTa) embeddings and (2) the number of atoms in the maximum common subgraph (MCS) of two molecules and their corresponding Euclidean distance in the embedding space.

5 Insights into MOLFORMER

In order to evaluate if MOLFORMER embeddings capture meaningful structural information, we performed the following experiments: First, we analysed the correlation between pairwise similarities estimated using the Tanimoto distance on the molecular fingerprints and those estimated using the Euclidean distance on the MOLFORMER embeddings. Second, we also looked into the correlation between the number of atoms in the maximum common subgraph of a pair of molecules and their corresponding euclidean distance in the embedding space. The results are summarized in Table 4 and show that MOLFORMER embeddings are better correlated with known molecule similarity measures when compared to ChemBERTa. Finally, we inspect the average pooled attention matrices. Figure 2 shows the average learned attention coefficients in an intermediate attention layer of MOLFORMER for two randomly selected molecules and compares those with the corresponding true chemical bonding patterns and the interatomic spatial distances(Complete attention matrices for more molecules and layers are shown in Appendix). We further compare absolute position embedding attention to the rotary one (relative). Visual inspection indicates

that an aggregation of heads on rotary intermediate attention layer better corresponds to the covalent bonding pattern, than its absolute counterpart. Interestingly, the rotary attention also shows signature of some of the long-range non-covalent interactions. This suggests that MOLFORMER indeed captures structural information.

6 Conclusion

In this work, we have explored the limit of large-scale pre-trained molecular language models for property prediction tasks in the context of molecular graph neural nets. Unlike graphs, molecular languages such as SMILES do not explicitly encode the molecular topology. However, with well-designed self-supervised training on a large-scale corpus and expressive architecture, such as a contextualized language model with an efficient linear attention mechanism, and a parallelized training protocol, our MOLFORMER can learn rich implicit structure-property relationship information.

References

1. Rogers, D. & Hahn, M. Extended-connectivity fingerprints. *J. chemical information modeling* **50**, 742–754 (2010).
2. Rupp, M., Tkatchenko, A., Müller, K.-R. & Von Lilienfeld, O. A. Fast and accurate modeling of molecular atomization energies with machine learning. *Phys. review letters* **108**, 058301 (2012).
3. Weininger, D. Smiles, a chemical language and information system. 1. introduction to methodology and encoding rules. *J. chemical information computer sciences* **28**, 31–36 (1988).
4. Goh, G. B., Hodas, N. O., Siegel, C. & Vishnu, A. Smiles2vec: An interpretable general-purpose deep neural network for predicting chemical properties. *arXiv:1712.02034* (2017).
5. Öztürk, H., Özgür, A. & Ozkirimli, E. Deepdta: deep drug–target binding affinity prediction. *Bioinformatics* **34**, i821–i829 (2018).
6. Paul, A. *et al.* Chemixnet: Mixed dnn architectures for predicting chemical properties using multiple molecular representations. *arXiv:1811.08283* (2018).
7. Shin, B., Park, S., Kang, K. & Ho, J. C. Self-attention based molecule representation for predicting drug-target interaction. In *Machine Learning for Healthcare Conference*, 230–248 (PMLR, 2019).
8. Daylight Chemical Information Systems, I. SmartsTM—a language for describing molecular patterns (2007).
9. Krenn, M., Häse, F., Nigam, A., Friederich, P. & Aspuru-Guzik, A. Self-referencing embedded strings (SELFIES): A 100% robust molecular string representation. *Mach. Learn. Sci. Technol.* **1**, 045024, DOI: [10.1088/2632-2153/aba947](https://doi.org/10.1088/2632-2153/aba947) (2020).
10. Jo, J., Kwak, B., Choi, H.-S. & Yoon, S. The message passing neural networks for chemical property prediction on smiles. *Methods* **179**, 65–72 (2020). Interpretable machine learning in bioinformatics.
11. Duvenaud, D. *et al.* Convolutional networks on graphs for learning molecular fingerprints. In *Proceedings of the 28th International Conference on Neural Information Processing Systems - Volume 2*, NIPS’15 (2015).
12. Defferrard, M., Bresson, X. & Vandergheynst, P. Convolutional neural networks on graphs with fast localized spectral filtering (2017). [1606.09375](https://arxiv.org/abs/1606.09375).
13. Kipf, T. N. & Welling, M. Semi-supervised classification with graph convolutional networks (2017). [1609.02907](https://arxiv.org/abs/1609.02907).
14. Li, Y., Tarlow, D., Brockschmidt, M. & Zemel, R. Gated graph sequence neural networks. *arXiv:1511.05493* (2015).
15. Veličković, P. *et al.* Graph attention networks. *arxiv*, [1710.10903](https://arxiv.org/abs/1710.10903) (2018).
16. Hamilton, W. L., Ying, R. & Leskovec, J. Inductive representation learning on large graphs (2018). [1706.02216](https://arxiv.org/abs/1706.02216).
17. Gilmer, J., Schoenholz, S. S., Riley, P. F., Vinyals, O. & Dahl, G. E. Neural message passing for quantum chemistry (2017). [1704.01212](https://arxiv.org/abs/1704.01212).
18. Schlichtkrull, M. *et al.* Modeling relational data with graph convolutional networks (2017). [1703.06103](https://arxiv.org/abs/1703.06103).
19. Liao, R., Zhao, Z., Urtasun, R. & Zemel, R. S. Lanczosnet: Multi-scale deep graph convolutional networks (2019). [1901.01484](https://arxiv.org/abs/1901.01484).
20. Chen, P., Liu, W., Hsieh, C.-Y., Chen, G. & Zhang, S. Utilizing edge features in graph neural networks via variational information maximization. *1906.05488* (2019).
21. Kirkpatrick, P. & Ellis, C. Chemical space. *Nature* **432**, 823–824 (2004).
22. Vaswani, A. *et al.* Attention is all you need. *arXiv:1706.03762* (2017).

23. Chithrananda, S., Grand, G. & Ramsundar, B. Chemberta: Large-scale self-supervised pretraining for molecular property prediction (2020). [2010.09885](#).
24. Wang, Y., Wang, J., Cao, Z. & Farimani, A. B. Molclr: Molecular contrastive learning of representations via graph neural networks (2021). [2102.10056](#).
25. Liu, Y. *et al.* Roberta: A robustly optimized bert pretraining approach. *arXiv:1907.11692* (2019).
26. Devlin, J., Chang, M.-W., Lee, K. & Toutanova, K. BERT: Pre-training of deep bidirectional transformers for language understanding. In *Proceedings of the 2019 Conference of the NAACL: HLT, Vol 1* (2019).
27. Raffel, C. *et al.* Exploring the limits of transfer learning with a unified text-to-text transformer. *JMLR* (2020).
28. Choromanski, K. *et al.* Rethinking attention with performers. *CoRR* **abs/2009.14794** (2020).
29. Beltagy, I., Peters, M. E. & Cohan, A. Longformer: The long-document transformer. *arXiv:2004.05150* (2020).
30. Kitaev, N., Kaiser, L. & Levskaya, A. Reformer: The efficient transformer. In *ICLR* (2020).
31. Wang, S., Li, B. Z., Khabsa, M., Fang, H. & Ma, H. Linformer: Self-attention with linear complexity (2020). [2006.04768](#).
32. Bjerrum, E. J. Smiles enumeration as data augmentation for neural network modeling of molecules (2017). [1703.07076](#).
33. Coley, C. W., Barzilay, R., Green, W. H., Jaakkola, T. S. & Jensen, K. F. Convolutional embedding of attributed molecular graphs for physical property prediction. *J. chemical information modeling* **57**, 1757–1772 (2017).
34. Xiong, Z. *et al.* Pushing the boundaries of molecular representation for drug discovery with the graph attention mechanism. *J. medicinal chemistry* (2019).
35. Morris, C. *et al.* Weisfeiler and leman go neural: Higher-order graph neural networks. In *AAAI*, vol. 33, 4602–4609 (2019).
36. Maron, H., Ben-Hamu, H., Serviansky, H. & Lipman, Y. Provably powerful graph networks (2020). [1905.11136](#).
37. Schütt, K. T. *et al.* SchNet: A continuous-filter convolutional neural network for modeling quantum interactions. In *NeurIPS* (2017).
38. Klicpera, J., Groß, J. & Günnemann, S. Directional message passing for molecular graphs (2020). [2003.03123](#).
39. Vig, J. *et al.* Bertology meets biology: Interpreting attention in protein language models. *arXiv:2006.15222* (2020).
40. Rives, A. *et al.* Biological structure and function emerge from scaling unsupervised learning to 250 million protein sequences. *bioRxiv* DOI: [10.1101/622803](#) (2020).
41. Elnaggar, A. *et al.* Prototrans: Towards cracking the language of life's code through self-supervised learning. *bioRxiv* DOI: [10.1101/2020.07.12.199554](#) (2021).
42. Xue, D. *et al.* X-mol: large-scale pre-training for molecular understanding and diverse molecular analysis. *bioRxiv* DOI: [10.1101/2020.12.23.424259](#) (2020).
43. Wang, S., Guo, Y., Wang, Y., Sun, H. & Huang, J. Smiles-bert: Large scale unsupervised pre-training for molecular property prediction. In *Proceedings of the 10th ACM-BCB* (2019).
44. Liu, S., Demirel, M. F. & Liang, Y. N-gram graph: Simple unsupervised representation for graphs, with applications to molecules (2019). [1806.09206](#).
45. Rong, Y. *et al.* Self-supervised graph transformer on large-scale molecular data (2020). [2007.02835](#).
46. Kim, S. *et al.* PubChem 2019 update: improved access to chemical data. *Nucleic Acids Res.* (2018).
47. Irwin, J. J. & Shoichet, B. K. ZINC—a free database of commercially available compounds for virtual screening. *J. Chem. Inf. Model.* **45**, 177–182 (2005).
48. Schwaller, P. *et al.* Molecular transformer: A model for uncertainty-calibrated chemical reaction prediction. *ACS Cent. Sci.* **5**, 1572–1583, DOI: [10.1021/acscentsci.9b00576](#) (2019).
49. Katharopoulos, A., Vyas, A., Pappas, N. & Fleuret, F. Transformers are rnns: Fast autoregressive transformers with linear attention. *CoRR* **abs/2006.16236** (2020). [2006.16236](#).
50. Shaw, P., Uszkoreit, J. & Vaswani, A. Self-attention with relative position representations. In *NAACL-HLT*, 464–468 (Association for Computational Linguistics, New Orleans, Louisiana, 2018).
51. Raffel, C. *et al.* Exploring the limits of transfer learning with a unified text-to-text transformer. *JMLR* **21**, 1–67 (2020).
52. Ke, G., He, D. & Liu, T.-Y. Rethinking positional encoding in language pre-training. In *ICLR* (2021).

53. Su, J., Lu, Y., Pan, S., Wen, B. & Liu, Y. Roformer: Enhanced transformer with rotary position embedding (2021). [2104.09864](#).
54. You, Y. *et al.* Large batch optimization for deep learning: Training bert in 76 minutes. *arXiv:1904.00962* (2019).
55. Wu, Z. *et al.* Moleculenet: A benchmark for molecular machine learning (2018). [1703.00564](#).
56. Lu, C. *et al.* Molecular property prediction: A multilevel quantum interactions modeling perspective. In *AAAI*, 1052–1060, DOI: [10.1609/aaai.v33i01.33011052](#) (AAAI Press, 2019).
57. Yang, K. *et al.* Analyzing learned molecular representations for property prediction. *J. Chem. Inf. Model.* **59**, 3370–3388 (2019).
58. Hu, W. *et al.* Strategies for pre-training graph neural networks (2020). [1905.12265](#).
59. Altae-Tran, H., Ramsundar, B., Pappu, A. S. & Pande, V. Low data drug discovery with one-shot learning. *ACS central science* (2017).
60. Rupp, M., Tkatchenko, A., Müller, K.-R. & von Lilienfeld, O. A. Fast and accurate modeling of molecular atomization energies with machine learning. *Phys. Rev. Lett.* **108**, 058301, DOI: [10.1103/PhysRevLett.108.058301](#) (2012).
61. Schütt, K. T., Arbabzadah, F., Chmiela, S., Müller, K. R. & Tkatchenko, A. Quantum-chemical insights from deep tensor neural networks. *Nat. communications* **8**, 1–8 (2017).
62. Vignac, C., Loukas, A. & Frossard, P. Building powerful and equivariant graph neural networks with structural message-passing (2020). [2006.15107](#).
63. Chen, T., Kornblith, S., Norouzi, M. & Hinton, G. A simple framework for contrastive learning of visual representations (2020). [2002.05709](#).
64. van den Oord, A., Li, Y. & Vinyals, O. Representation learning with contrastive predictive coding (2019). [1807.03748](#).

Supplementary Material: Do Large Scale Molecular Language Representations Capture Important Structural Information?

A Appendix

We give here additional details and experiments to support our findings in the paper.

B Training Details

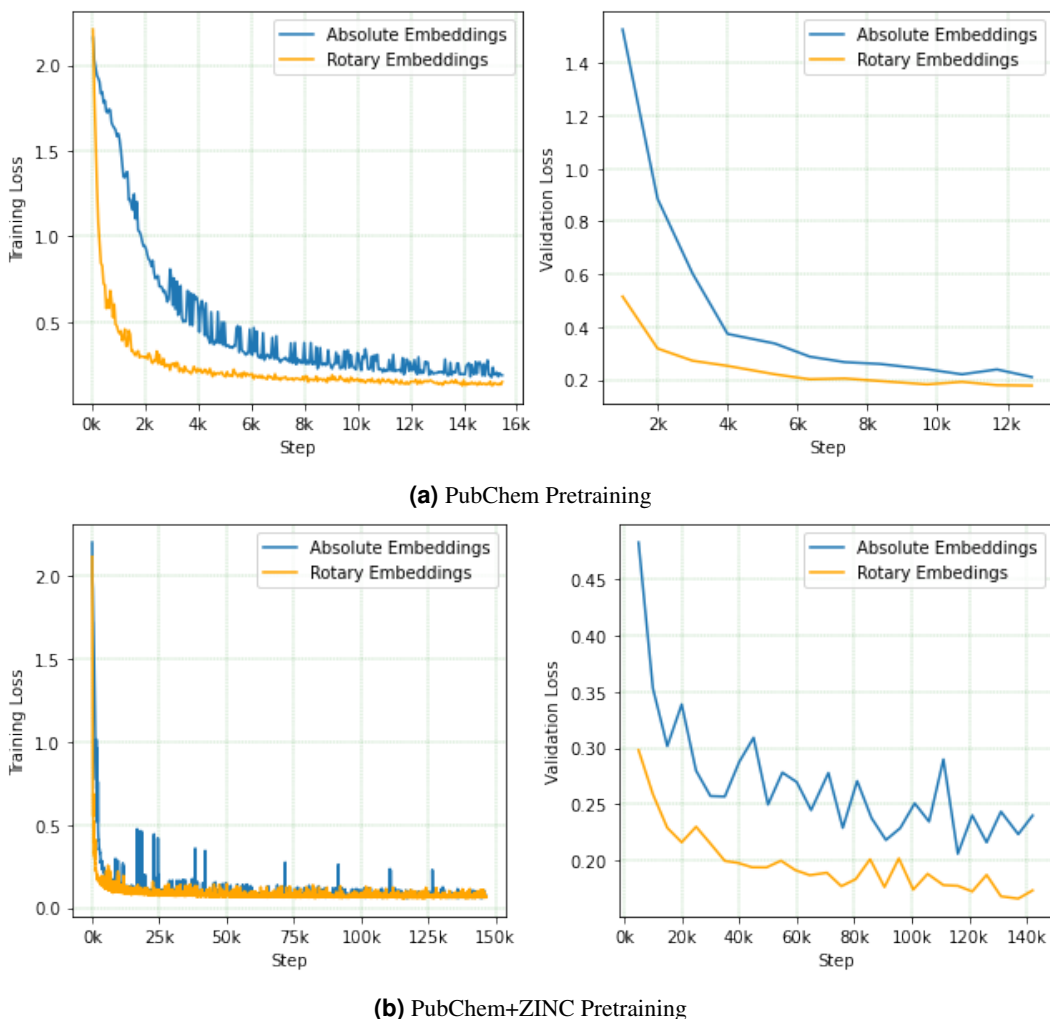


Figure 3. Training and validation losses of our Linear attention MOLFORMER with *rotary* (relative) and absolute position embeddings on a) PubChem and b) PubChem+ZINC (>1 billion data points). We see that both rotary and absolute MOLFORMER have graceful training curves. Our Rotary Linear attention MOLFORMER leads to lower training and validation losses than MOLFORMER with absolute position embeddings.

Faster Training with Adaptive Bucketing By Sequence Length We observed that the distribution of molecule lengths in our dataset centered around molecules that were less than 45 characters long after tokenization. This fact coupled with large batch sizes increased the likelihood that padding tokens would overwhelm each batch and result in large amounts of computational waste. To address this problem we decided to break each minibatch into multiple buckets. This process is done on a batch by batch basis, i.e. on the fly, which means full dataset preprocessing does not take place. It should be noted that gathering of statistics for the full dataset did take place before training and buckets were defined by sequence interval length gathered from that process. The first bucket would contain SMILES strings of length 1 to 42, the next bucket would be of size 43 to 66, the third bucket would be of size 67 to 122 and finally the last bucket would be of size 123 to 202. Due to the length

Pretraining Data →	Pubchem Only			PubChem+ZINC		
Measure ↓	Frozen × Rotary	Finetuned × Rotary	Finetuned ✓ Rotary	Frozen × Rotary	Finetuned × Rotary	Finetuned ✓ Rotary
α	1.5470	0.5280	0.8452	0.5312	0.3713	0.3327
C_v	0.9984	0.1506	0.2701	0.2303	0.1584	0.1447
G	2.0089	0.8626	1.5920	0.3066	0.6861	0.3362
gap	0.0182	0.0050	0.0109	0.0036	0.0039	0.0038
H	2.3627	1.3342	0.7088	0.3675	.07369	0.2522
ϵ_{homo}	0.0147	0.0038	0.0082	0.0062	0.0028	0.0029
ϵ_{lumo}	0.0148	0.0036	0.0080	0.0058	0.0025	0.0027
μ	0.8509	0.4284	0.6166	0.6463	0.3921	0.3616
$\langle R^2 \rangle$	87.2816	30.2904	34.0425	27.5962	18.8286	17.0620
U_0	2.0613	0.8969	1.5503	0.4500	0.4244	0.3211
U	1.9638	1.1122	1.1351	0.4480	0.7370	0.2522
ZPVE	0.0020	0.0008	0.0012	0.0004	0.0002	0.0003
Avg MAE	8.260	2.968	3.3990	2.5497	1.8620	1.5894
Avg std MAE	0.2447	0.0801	0.1355	0.0978	0.0611	0.0567
# Wins for fixed data	0	11	1	2	3	7

Table 5. Comparison of different MOLFORMER variants on QM9 test set. Models on the left half of the table are pre-trained using QM9 only, whereas the models on the right half are pre-trained on the PubChem+ZINC dataset. The variants with (✓) and without (×) rotary embeddings are compared. Our best candidate variant (for Table 1) is picked based on the average MAE score.

distribution of our dataset buckets 1 and 2 would always be present in all training steps while bucket 3 would be present for the majority of minibatches. Molecules that fell into bucket 4 appeared in most minibatches but would usually only represent a very small percentage of molecules found within the minibatch. With this information we decided to not utilize bucket 4 in the training procedure until it reached a threshold of 50 molecules thus preventing us from training on a bucket that consistently contained a very small amount of molecules which we believe aided training. Bucketing combined with gradient accumulation across buckets gave us stable training, maintained training randomization and reduced computational time needed compared to the traditional method of keeping GPU memory full at all times to maximize computation without consideration of the wasted computation that arises because of the large amount of padding tokens. To be more concrete, without bucketing on 1 V100 GPU and on PubChem only a single epoch would take approx. 1200 hours while with bucketing the same epoch only took around 60 hours giving adaptive bucketing a speedup of $3.3\times$. A similar concept, namely micro-batching exists but we became aware of it after implementing our adaptive bucketing technique. We have not yet baselined the differences between our domain specific bucketing implementation towards molecular data and the generic micro-batching. .

Using Linear attention and bucketing allowed us to reduce the number of GPUs needed for quadratic attention and no bucketing from roughly 1000 to 16.

Parallelization and Computing Environment All experiments were performed on a GPU cluster where each node contains either 8 NVIDIA Tesla V100 (32GB) or 8 Ampere A100 (40GB) GPUs connected via NVLink. The V100 nodes are equipped with dual 28-core (Intel Xeon Gold 6258R) CPUs, the A100 nodes are equipped with dual 64-core (AMD EPYC 7742) CPUs, and all nodes are connected by 2 non-blocking EDR InfiniBand (100Gbps) network adapters as well as 2 100Gbps Ethernet adapters. All nodes are installed with RHEL 8.3, CUDA 10.2, and cuDNN 7.5.

Due to the size of the datasets utilized in pretraining, our training environment relies on the Distributed Data Parallel functions provided by Pytorch and Pytorch Lightning utilizing the NCCL backend. By utilizing RDMA to enable GPU-direct technology we were able to efficiently scale to multi-node multi-GPU training. Additionally, we utilized HuggingFace Datasets to localize the data onto the machines where pretraining took place to improve performance during pretraining. Our pretraining task consists of training on the full dataset to 4 epochs. Training a single epoch of just PubChem on a single NVIDIA V100 GPU would take approximately 60 hours. Utilizing Distributed Data Parallel, pretraining on the full PubChem dataset alone took approx. 22 hours on 16 NVIDIA V100 GPUs this averages to about 5.5 hours per epoch. The speed up achieved by parallelizing training to 16 GPUs gave us a factor of 10.9. Pretraining for 4 epochs on the combined PubChem+ZINC datasets took approx 208 hours on a 16 NVIDIA V100 GPUs which averages to about 52 hours of compute for a single epoch. All finetuning tasks were able to be performed on single GPUs (either V100 or A100) and completed in approx. 12 hours.

C Mean and Standard Deviation for Prediction Results Across Different Data Folds

The two major high-level variants of MOLFORMER are based on whether the weights of the base MOLFORMER are frozen or if the weights are trained during the finetuning process on downstream tasks. Throughout the paper, these setups are referred to as either ‘Frozen’ or ‘Finetuned’, respectively.

We report the mean and standard deviations of MAE for 5 different folds of the data split into 80% training and 10% validation and 10% test. Most of the related work does not perform cross validation and just report the results on a single split. We note that the standard deviations are quite low for most of the predictions and the mean errors are in line with the main paper for all folds of all tasks which suggests the MOLFORMER representations are robust.

PubChem Only				
Measure ↓	Frozen × Rotary	Frozen ✓ Rotary	Finetuned × Rotary	Finetuned ✓ Rotary
α	1.5915 ± 0.0413	1.4379 ± 0.0168	0.6661 ± 0.0685	0.6575 ± 0.0509
C_v	0.9852 ± 0.0261	0.8995 ± 0.0269	0.1641 ± 0.0665	0.1607 ± 0.0058
G	1.7218 ± 0.1061	2.3068 ± 0.1276	1.2877 ± 0.3059	1.4234 ± 0.2985
gap	0.0182 ± 0.0003	0.0174 ± 0.0002	0.0052 ± 0.0002	0.0051 ± 0.0001
H	2.2200 ± 0.0652	2.1615 ± 0.2438	1.3401 ± 0.2877	1.4220 ± 0.3053
ϵ_{homo}	0.0115 ± 0.0001	0.0111 ± 0.0001	0.0036 ± 0.0005	0.0036 ± 0.0001
ϵ_{lumo}	0.0148 ± 0.0002	0.0141 ± 0.0001	0.0034 ± 0.0001	0.0033 ± 0.0001
μ	0.8670 ± 0.0212	0.8505 ± 0.0157	0.4210 ± 0.0043	0.4257 ± 0.0083
$\langle R^2 \rangle$	87.6172 ± 1.7076	77.5032 ± 1.4228	24.3940 ± 2.1510	24.9213 ± 2.5526
U_0	1.9149 ± 0.1942	1.9247 ± 0.0941	1.3295 ± 0.2696	1.4516 ± 0.2722
U	1.8106 ± 0.1409	1.7770 ± 0.1462	1.3926 ± 0.1379	1.3366 ± 0.3006
ZPVE	0.0021 ± 0.0002	0.0017 ± 0.0001	0.0008 ± 0.0001	0.0008 ± 0.0001

Table 6. Mean and standard deviation of Mean Absolute Error (MAE) on the various QM9 tasks using a pretrained model that is trained on PubChem only.

PubChem+Zinc				
Measure ↓	Frozen × Rotary	Frozen ✓ Rotary	Finetuned × Rotary	Finetuned ✓ Rotary
α	0.6468 ± 0.0169	1.2956 ± 0.0244	0.4246 ± 0.0486	0.3455 ± 0.0066
C_v	0.2825 ± 0.0078	0.7959 ± 0.0141	0.2080 ± 0.0340	0.1589 ± 0.0102
G	1.2865 ± 0.1192	2.1535 ± 0.0503	0.7696 ± 0.0719	0.3609 ± 0.0276
gap	0.0089 ± 0.0000	0.0165 ± 0.0002	0.0038 ± 0.0001	0.0040 ± 0.0001
H	1.0730 ± 0.3188	1.8490 ± 0.1469	0.8525 ± 0.0855	0.3318 ± 0.0512
ϵ_{homo}	0.0066 ± 0.0000	0.0103 ± 0.0001	0.0030 ± 0.0001	0.0029 ± 0.0001
ϵ_{lumo}	0.0063 ± 0.0000	0.0128 ± 0.0001	0.0039 ± 0.0002	0.0029 ± 0.0001
μ	0.6872 ± 0.0049	0.8089 ± 0.0205	0.3986 ± 0.0060	0.3709 ± 0.0065
$\langle R^2 \rangle$	29.3779 ± 0.2944	72.8752 ± 1.1180	19.9005 ± 0.3305	17.8121 ± 0.8596
U_0	1.2877 ± 0.2373	2.1030 ± 0.0967	0.8492 ± 0.1102	0.3795 ± 0.0820
U	1.3238 ± 0.1954	1.8647 ± 0.0601	0.8631 ± 0.0999	0.3677 ± 0.0382
ZPVE	0.0005 ± 0.0000	0.0018 ± 0.0001	0.0003 ± 0.0001	0.0003 ± 0.0001

Table 7. Mean and standard deviation of Mean Absolute Error (MAE) on the various QM9 tasks using a pretrained model that is trained on both Pubchem and Zinc

D Assets and License

The following table summarizes the libraries utilized for our experiments and their accompanying license terms.

Asset	License	Link
Fast-Transformers	MIT License	https://github.com/idiap/fast-transformers/blob/master/LICENSE
Pytorch	BSD Style License	https://github.com/pytorch/pytorch/blob/master/LICENSE
RDKit	BSD 3-Clause "New" or "Revised" License	https://github.com/rdkit/rdkit/blob/master/license.txt
Pytorch Lightning	Apache 2.0 License	https://github.com/PyTorchLightning/pytorch-lightning/blob/master/LICENSE
HuggingFace Datasets	Apache 2.0 License	https://github.com/huggingface/datasets/blob/master/LICENSE
Nvidia APEX	BSD 3-Clause "New" or "Revised" License	https://github.com/NVIDIA/apex/blob/master/LICENSE

E Hyperparameters for Property Prediction

During the finetuning process, where the MOLFORMER weights are not frozen, we experimented with different hyperparameters. In our experiments, we found that batch sizes of both 64 and 128 work best for the downstream tasks. Also, among various learning rates, $3e-5$ seems to be the best fit for all the measures on QM9 dataset. We found that the beta values used by the optimizer were important and were set to β_1 equaling .9 and β_2 equaling .99. We found the model to be very sensitive to the β_2 value during fine tuning. The discriminator used was of a fixed size of 2 layers with a hidden size of 768 for all fine tuning experiments.

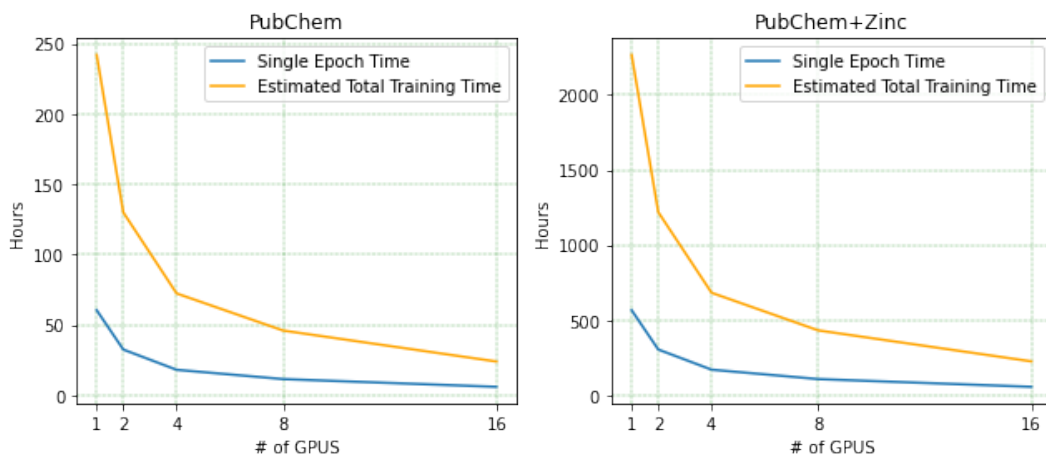
For the frozen strategy where the embeddings from the MOLFORMER are fixed, we use a fully connected model to predict the properties. A hyperparameter sweep was performed for the frozen strategy using grid search and we randomly picked 25 different variations for each task. The best model with the lowest validation loss was picked for further analysis. The different values of the frozen strategy hyperparameters are summarized in the table below.

Table 8. Different Values of the hyperparameters for the Frozen Models

Hyperparameter	Values
Learning Rate	0.001, 0.0001, 0.0005, 0.00005
Batch Size	64, 128, 256
Hidden Dimension	64, 128, 256, 512, 1024
Number of Layers	2, 3, 4

F PreTraining Scaleout

We give in Figure 1 the estimated training times of MOLFORMER as a function of the used GPUs in the parallelization.



(a) Estimated Pretraining Time

Figure 4. Estimated training times for our Linear attention MOLFORMER with *rotary* embeddings on a) PubChem and b) PubChem+ZINC datasets taken after 250 iterations. We see that training time decrease slightly sub-linearly as GPUs are added. Training time also scales approximately linearly as more data is added.

G Dataset, Vocabulary and Units

All our downstream evaluations are performed on tasks from the Moleculenet dataset⁵⁵. All the tasks mentioned in Table 2 use random splits as suggested in⁵⁵, while those in Table 3 use scaffold splits as suggested in²⁴. We refer the reader to⁵⁵ for more details on the specific tasks.

We have observed that various related work in the past have used different units for quantitative analysis on QM9 dataset without explicitly stating the units, making it difficult to compare the relative performance of different methods. We have listed the units of the measures used in this paper in Table 9. We also give in Tables 10 and 11 the statistics of sequence length and vocabulary for the datasets considered in this work.

Measure	Unit
α	Bohr ³
C_v	cal/(mol*K)
G	Hartree
gap	Hartree
H	Hartree
ϵ_{homo}	Hartree
ϵ_{lumo}	Hartree
μ	Debye
$\langle R^2 \rangle$	Bohr ²
U_0	Hartree
U	Hartree
ZPVE	Hartree

Table 9. Units of QM9 target measures

Table 10. Minimum, maximum and mean and standard deviation of sequence length for the datasets considered in this work. The vocabulary size after tokenization is also given in the last column.

Pretrained Data	Min	Max	Mean	Std	Vocab Size
QM9	1	22	14.76	2.02	30
Pubchem	1	2211	49.13	24.90	2252
Zinc	4	152	43.08	8.70	113
Pubchem + Zinc	1	2211	44.76	14.55	2279

Table 11. Top five most frequent tokens for each data source.

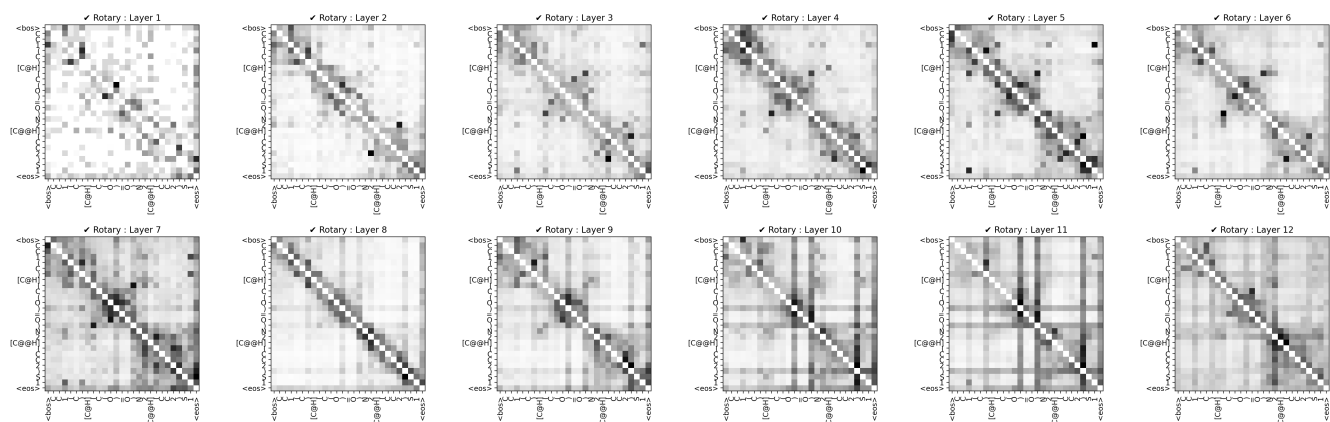
Pretrained Data	Most Frequent Tokens
QM9	C, 1, 0, 2, (
Pubchem	C, =, (,), 0
Zinc	C, c, (,), 1
Pubchem + Zinc	C, c, (,), =

Pretraining Data →	QM9 Only			PubChem+ZINC		
Measure ↓	Frozen × Rotary	Finetuned × Rotary	Finetuned ✓ Rotary	Frozen × Rotary	Finetuned × Rotary	Finetuned ✓ Rotary
α	1.6258	0.5078	0.6001	0.5312	0.3713	0.3327
C_v	1.0176	0.1589	0.1906	0.2303	0.1584	0.1447
G	3.2528	0.9985	0.7479	0.3066	0.6861	0.3362
gap	0.0187	0.0057	0.0061	0.0036	0.0039	0.0038
H	1.9221	1.1579	1.0250	0.3675	.07369	0.2522
ϵ_{homo}	0.0115	0.0042	0.0046	0.0062	0.0028	0.0029
ϵ_{lumo}	0.0157	0.0041	0.0056	0.0058	0.0025	0.0027
μ	0.8394	0.4380	0.4630	0.6463	0.3921	0.3616
$\langle R^2 \rangle$	86.9461	24.0785	25.9482	27.5962	18.8286	17.0620
U_0	3.0626	1.1462	1.3168	0.4500	0.4244	0.3211
U	1.8555	1.0454	1.6158	0.4480	0.7370	0.2522
ZPVE	0.0020	0.0011	0.0012	0.0004	0.0002	0.0003
Avg MAE	8.3808	2.4621	2.6604	2.5497	1.8620	1.5894
Avg std MAE	0.2390	0.0843	0.0937	0.0978	0.0611	0.0567
# Wins for fixed data	0	10	2	2	3	7

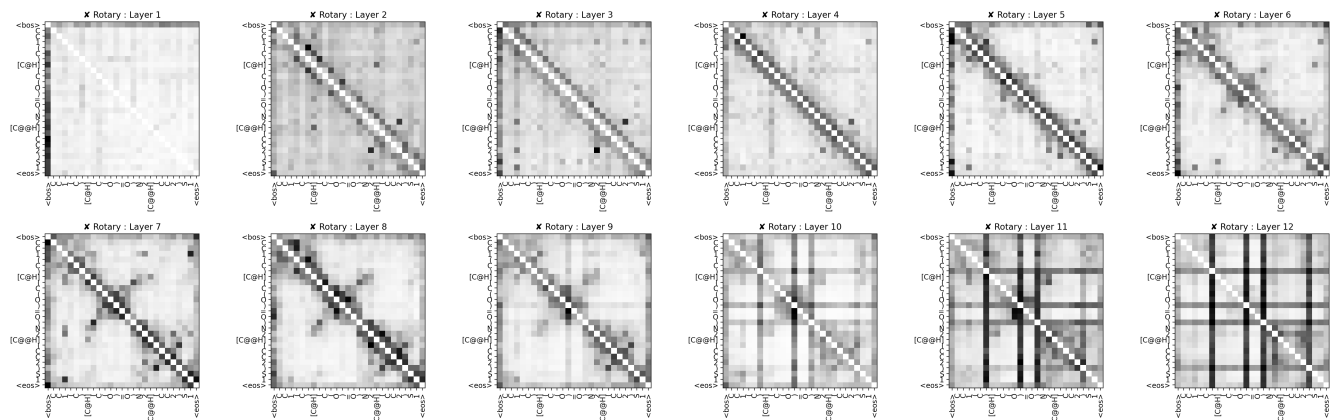
Table 12. Comparison of different MOLFORMER variants on the QM9 test set. Models on the left half of the table are pre-trained using QM9 only, whereas the models on right half are pre-trained on the PubChem+ZINC dataset. The variants with (✓) and without (×) rotary embeddings are compared. Our best candidate variant (for Table 1) is picked based on the average MAE score.

H Attention and Structure

In this section we present a visual comparison to show the attention representations of three random molecules generated by the rotary and non-rotary models. The attention head weights of each layer are averaged and all layers are presented in figures 5, 6, 7. Several interesting observations can be made from these representations. For both rotary and its absolute counterpart, in higher layers (layer 9 and up), most of attentions are directed toward the closing parentheses. Therefore, it is reasonable to avoid those layers for identifying meaningful features. For the non-rotary model, the first attention layer seems to be very similar for all molecules, the only noticeable feature is high attention on BOS and EOS tokens. Given that the first layer of the non-rotary model is almost deterministic in its representation, it is possible that the representation is not determined by the molecule but the architecture itself. In contrast, the first layer of the rotary model representation seems to be heavily influenced by the molecule. For both models, intermediate layers (layer 5-7) indicate learning of the SMILES grammar, such as high attention between opening and closing parentheses. In those layers, representations learned by the rotary model are more distinctive and reminiscent of the covalent and non-covalent interactions within a molecule, when compared to its non-rotary counterpart. While the performance between the rotary and non rotary models have been similar with respect to our evaluation on downstream tasks the differences in their attention weights and in discovering structural information from SMILES representation is insightful and intriguing on the impact of position embedding in capturing the structural information of molecules.

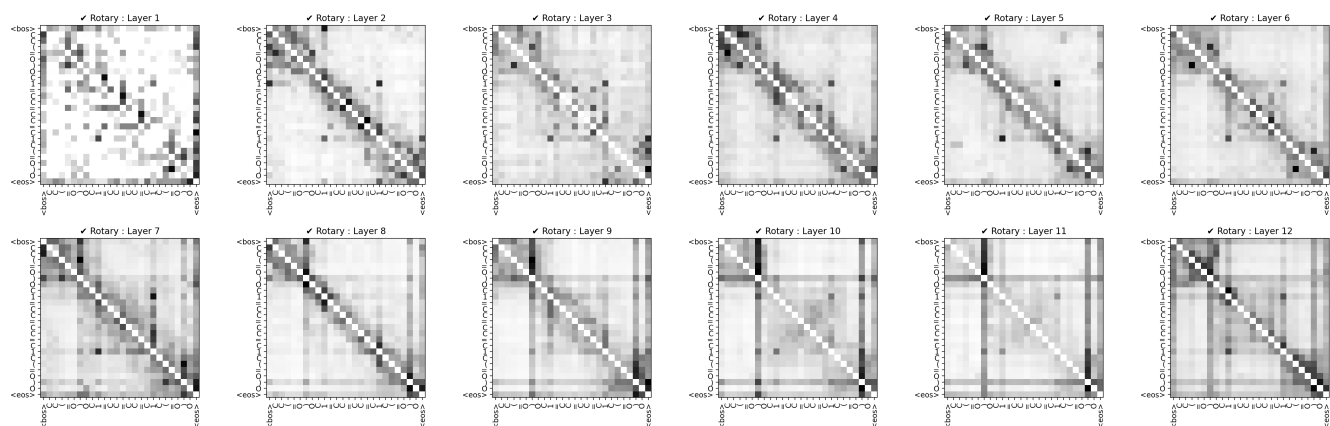


(a) Attention Map for rotary/relative embedding variant of MoLFORMER

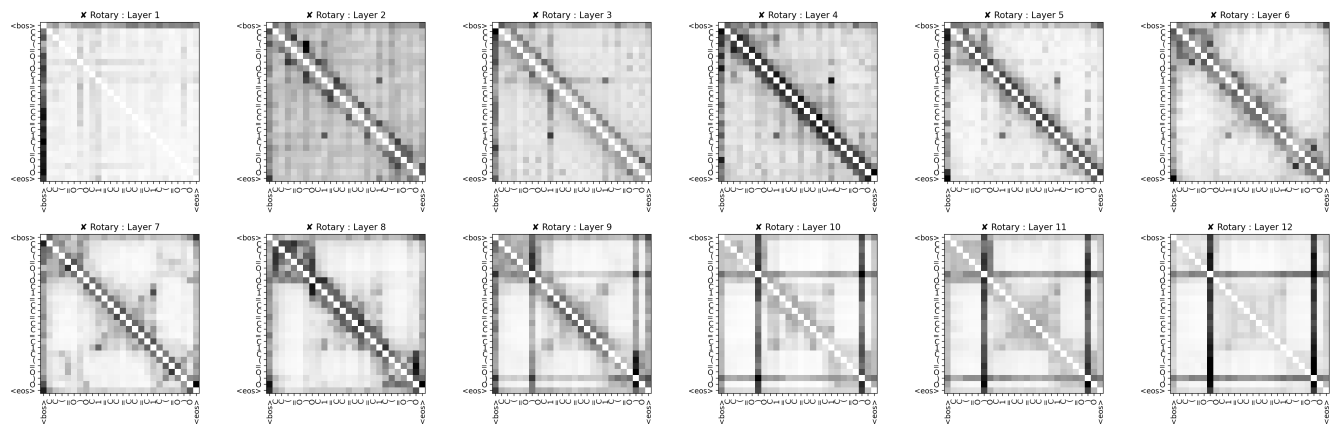


(b) Attention Map for non-rotary/absolute embedding variant of MoLFORMER

Figure 5. Attention map shown for the smile sequence 'CC1 (C) [C@H] (C (O) =O) N2 [C@@H] (CC2) S1' for all the layers of MoLFORMER. For each layer, the attentions are average-pooled across all the heads.



(a) Attention Map for rotary/relative embedding variant of MoLFORMER



(b) Attention Map for non-rotary/absolute embedding variant of MoLFORMER

Figure 6. Attention map shown for the smile sequence 'CC(=O)OC1=CC=CC=C1C(=O)O' for all the layers of MoLFORMER. For each layer, the attentions are average-pooled across all the heads.

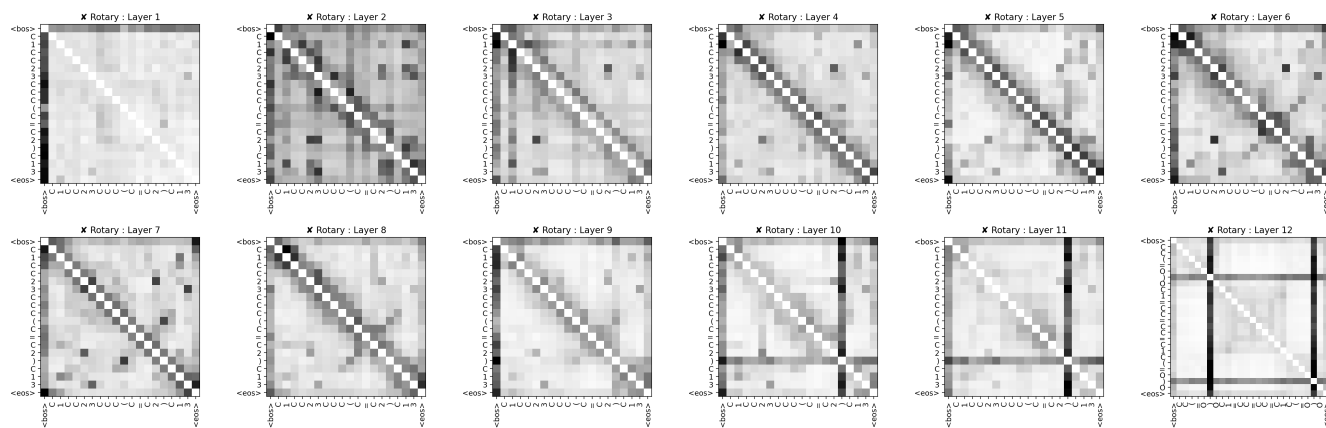
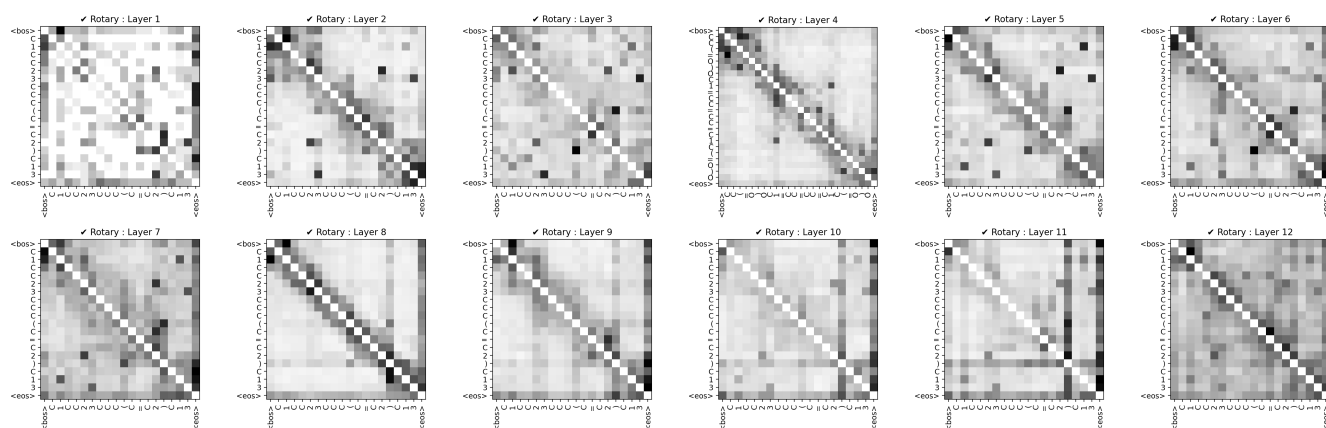


Figure 7. Attention map shown for the smile sequence ``C1CC23CCC (C=C2) C13'` for all the layers of MoLFormer. For each layer, the attentions are average-pooled across all the heads.